Nanotechnology **20** (2009) 285305 (6pp) doi:10.1088/0957-4484/20/28/285305

Filling of hole arrays with InAs quantum dots

Jennifer Y Lee[1], Mark J Noordhoek[1], Peter Smereka[2], Hugh McKay[1] and Joanna M Millunchick[1]

[1] Department of Materials Science and Engineering, University of Michigan, Ann Arbor, MI 48109, USA
[2] Department of Mathematics, University of Michigan and the Michigan Center for Theoretical Physics, Ann Arbor, MI 48109, USA

Received 16 April 2009, in final form 21 May 2009
Published 23 June 2009
Online at stacks.iop.org/Nano/20/285305

Abstract
Focused ion beams are used to pattern GaAs(001) surfaces with an array of nanometer-deep holes upon which deposition of InAs results in quantum dot formation at the hole location. Experiments show that the size and quantity of quantum dots formed depend on growth parameters, and ion dose, which affects the size and shape of the resulting holes. Quantum dots fabricated in this fashion have a photoluminescence peak at 1.28 eV at 77 K, indicating that the ion irradiation due to patterning does not destroy their optical activity. Kinetic Monte Carlo simulations that include elastic relaxation qualitatively model the growth of dots in nanometer-deep holes, and demonstrate that growth temperature, depth of the holes, and the angle of the hole sidewalls strongly influence the number of quantum dots that form at their perimeter.

(Some figures in this article are in colour only in the electronic version)

1. Introduction

The alignment of InAs quantum dots into regular and dense arrays has been vigorously pursued for applications in optoelectronics [1, 2] and cryptography [3, 4]. A variety of schemes to control the nucleation locations of the dots have been examined, ranging from standard lithographic techniques [5–7] to atomic force lithography [8]. *In situ* focused ion beam (FIB) patterning has the capability of creating patterns on the order of a few hundred nanometers or less, without the need for *ex situ* processing [9–11]. As such, FIB patterning has emerged as a viable tool for the fabrication of photonic and optoelectronic devices [12, 13]. In order to make use of these patterns in device applications, the resulting quantum dot arrays must be regular and uniform and retain their optical activity. In this paper, we examine the effect of the FIB patterning of GaAs substrates on the assembly of InAs quantum dots and show that they luminesce. Experiments show that the regularity of the resulting quantum dot arrays is most strongly dictated by the fidelity of the initial pattern of holes. A unique kinetic Monte Carlo simulation of the growth that includes elastic relaxation of the lattice shows that the location, size, and number of dots can be delicately tuned by controlling the growth conditions and the geometry of patterned hole.

2. Experimental details

In vacuo FIB patterning was used to direct the self-assembly of quantum dot arrays. Samples were grown using a molecular beam epitaxy system on GaAs(001) substrates. Typical values for growth rates were 0.75 monolayers s^{-1} (ML s^{-1}) for Ga, and 0.25 ML s^{-1} for In. Two different As_4 fluxes, ∼1.0 and ∼2.2 ML s^{-1}, were employed to give similar III/V flux ratios while growing GaAs or InAs. All temperature measurements were made by an optical pyrometer. After oxide desorption, a 400 nm GaAs buffer layer was grown under the higher As_4 flux at a substrate temperature of $T = 580\,^{\circ}C$. The sample was then annealed at the growth temperature under a high As_4 flux and allowed to cool to room temperature under low arsenic flux. When cool, the sample was transferred *in vacuo* to the FIB patterning system. The FIB was employed to pattern the GaAs substrate with arrays of holes with 200–500 nm spacing. Each hole was dosed in a single pass with a 30 keV, 7.5 pA beam using ion dwell times ranging from 400 $\mu s \leqslant t \leqslant 1600\ \mu s$, which have predicted sputter depths on the order of a few monolayers or less [14]. After irradiation, samples were returned to the growth chamber and the sample temperature was raised to $T = 530\,^{\circ}C$ under low As_4 flux. Because the sample never left the vacuum system,

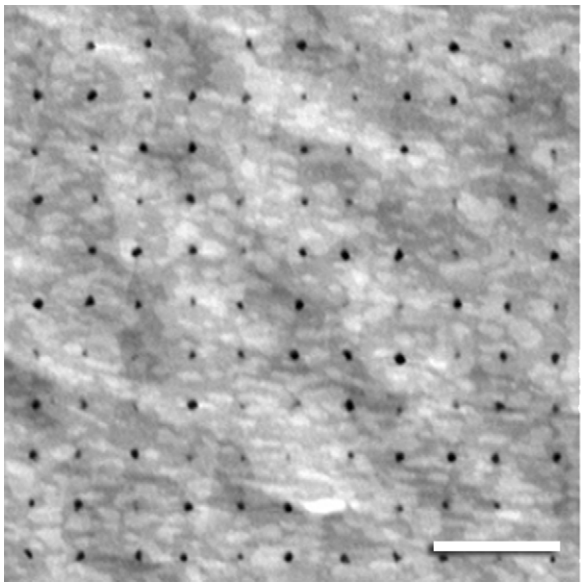

Figure 1. AFM images of a GaAs buffer layer that has been patterned with an array of holes spaced 250 nm apart and dosed with a dwell time of 800 μs per hole, followed by annealing at $T = 530\,^{\circ}$C under low As_4 flux. The scale bar is 500 nm, and the height scale in 3 nm.

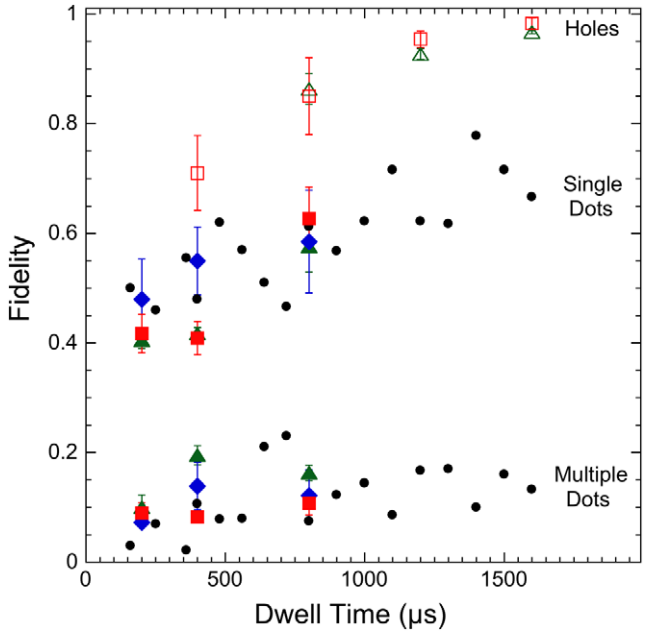

Figure 2. Probability of finding a hole, single quantum dot, or multiple quantum dots appearing at the intended location for a 2.0 ML-thick InAs film deposited at $T = 530\,^{\circ}$C for arrays with periodicity of 140 nm (green triangle), 275 nm (red square), 500 nm (black circle), and 550 nm (blue diamond).

issues often observed with regard to preferential oxidation of ion-irradiated areas [15, 16] are circumvented. Thin layers of InAs (1.7 ML $< h <$ 2.4 ML) were deposited at $T = 510$ or $530\,^{\circ}$C under a low arsenic flux while the surface had a $c(4\times4)$ reconstruction according to reflection high energy electron diffraction. Following growth, samples were quenched to

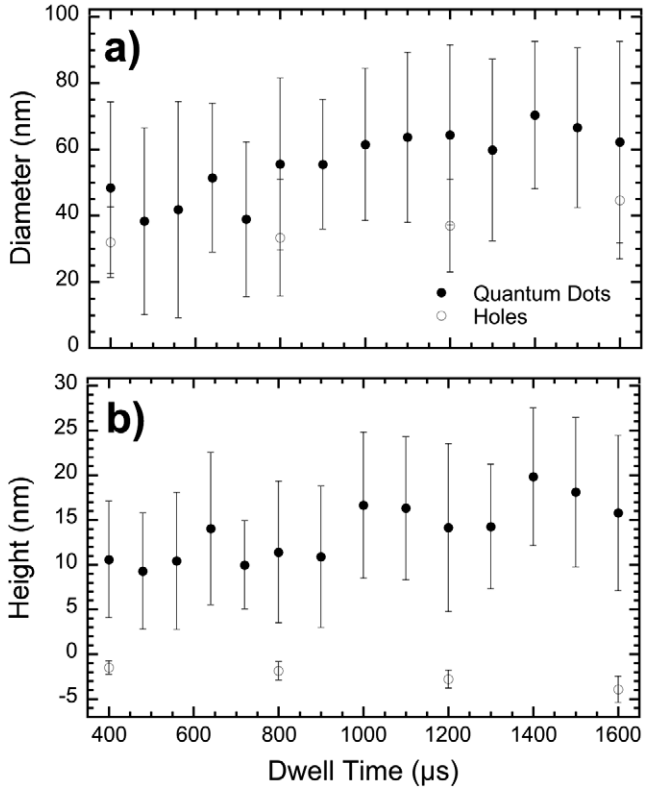

Figure 3. Plot of the feature (a) diameter and (b) height as a function of dwell time for holes (open circles) and quantum dots (closed circles).

room temperature under low As_4 flux. The samples were characterized *ex situ* using an atomic force microscope (AFM) in tapping mode, using tips with a radius of curvature of 8 nm.

3. Results and discussion

Figure 1 shows an AFM image of a GaAs buffer layer that has been patterned with an array of holes spaced 250 nm apart and dosed with a dwell time of 800 μs per hole followed by an anneal to $T = 530\,^{\circ}$C under low As_4 flux. For this set of patterning conditions, individual holes due to ion irradiation are clearly observed that are 42 $\pm$ 13 nm in diameter and 1.7 $\pm$ 0.7 nm deep. The step structure of the substrate is also resolved between the holes and is apparently unperturbed by the patterning process. The hole size varies, and in some instances no hole is visible at the expected location. The probability of finding a hole at the intended location, which we call the fidelity, increases as a function of ion dose (plotted in figure 2) and approaches 1 for the highest dwell times (1600 μs). The periodicity of the hole array does not affect the probability of finding a dot at the intended location for this set of irradiation conditions. The fact that at lower dwell times the fidelity is not unity suggests that the hole formation process has a stochastic component. Indeed, it has been shown that the Ga^+ ion beam initially injects point defects into the surface, which then coalesce into either a hole or an annular ring upon annealing [17]. It is possible that the beam conditions may still be optimized in order to improve the probability that exposure

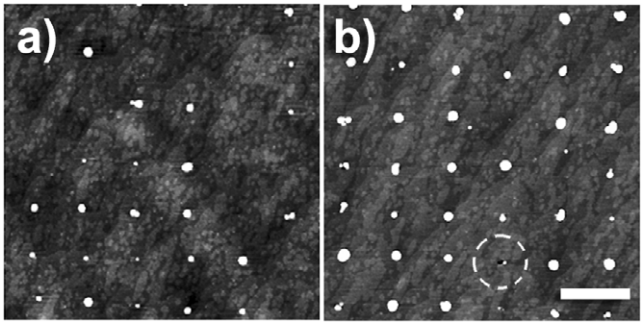

Figure 4. AFM images of a 2.0 ML InAs film deposited at $T = 530\,^{\circ}\mathrm{C}$ on GaAs upon hole arrays patterned 250 nm apart and at dwell times of (a) 560 μs and (b) 1500 μs. The scale bar is 500 nm, and the height scale is 10 nm in (a) and (b). The dotted circle in (b) indicates the presence of a quantum dot next to the irradiated hole it nucleated from.

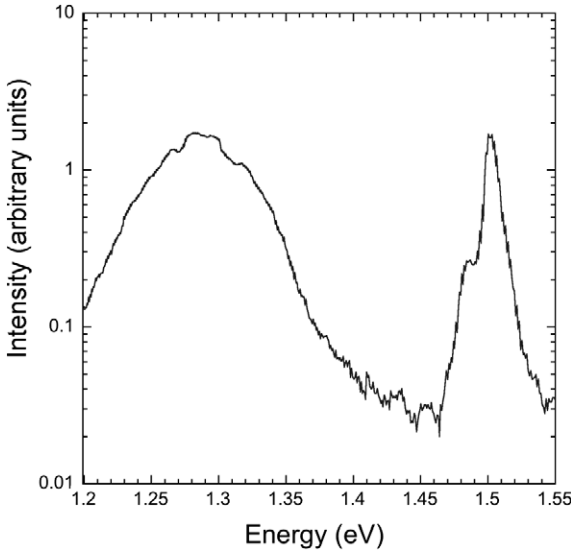

Figure 5. Photoluminescence spectra of FIB-modified surface. PL was performed at 77 K at a power of 15 mW.

to the ion beam will produce the desired feature with 100% fidelity at lower dwell times. The size of the holes increases with increasing dose. The open symbols in figure 3(a) show that the diameter of the holes increases from 30 ± 10 to 40 ± 18 nm as the dwell time changes from 400 to 1600 μs. The depth increases from 1.5 ± 1 to 4 ± 2 nm over the same range in ion dose (open symbols in figure 3(b)). However, it should be noted that when the holes become very narrow and deep, AFM is limited in its ability to accurately measure their true depth.

Growth of InAs upon these patterns results in the formation of regular arrays of quantum dots with a separation dictated by the dimensions of the pattern. Figures 4(a) and (b) show AFM micrographs of a 2.0 ML InAs film deposited at $T = 530\,^{\circ}\mathrm{C}$ upon hole arrays, patterned using various dwell times, 560 μs (figure 4(a)) and 1500 μs (figure 4(b)). In general, dots nucleate on the sites where the holes were patterned, and the probability of having a single quantum dot at the expected location increases with longer dwell time, as shown in figure 2. In some instances, the hole is still visible next to a quantum dot (circled in figure 4(b)). The probability of the formation of a single dot is lower than that of a hole for any given dwell time, but roughly follows the same slope. There is also a non-zero probability of finding more than one dot at the intended location, which increases somewhat with increasing dwell time. The number of dots increases with dwell time. A dwell time of 800 μs yields an average of 1.9 ± 0.9 dots, and a dwell time of 2000 μs yields an average of 5.8 ± 1.2 dots, which were tabulated from AFM images of one sample of 1.8 ML InAs grown at 510 °C on a FIB-irradiated surface with holes spaced 560 nm apart. For any given dwell time, the average quantum dot diameter is somewhat larger (64 ± 29 nm at 800 μs) than the average hole diameter (42 ± 13 nm at 800 μs), and weakly increases with increasing ion dose (closed symbols in figure 3).

The ratio of the height to the diameter of the FIB-induced quantum dots is 0.25 regardless of the dwell time. This compares favorably to reported aspect ratios of 0.24 and absolute sizes of quantum dots self-assembled without patterning [18]. This data shows that the ion irradiation or presence of any residual Ga^{+} from the ion beam has no effect on the surface energy of the system, contrary to observations of FIB-induced quantum dots in the SiGe system [19]. If the ion beam did alter the surface energy, due to deposition of excess Ga from the beam for instance, then the aspect ratio of the FIB-induced islands would be expected to be different than self-assembled islands.

Samples for micro-photoluminescence (PL) were also grown to examine the optical activity of the FIB-directed quantum dots. These samples were grown similar to those described above, except a 10 period 2.5 nm GaAs/2.5 nm AlAs superlattice was deposited prior to the quantum dot layer in order to amplify the PL emission, followed by a 10 nm GaAs spacer layer that was patterned by the FIB. The samples were then placed back into the chamber, and 1.8 ML InAs was deposited at $T = 510\,^{\circ}\mathrm{C}$ and capped with 10 nm GaAs. PL measurements were made *ex situ* with the sample mounted in a continuous-flow cryostat cooled to 77 K with liquid nitrogen. A 532 nm continuous-wave pump laser was focused with a 50× objective lens onto the FIB-irradiated regions. A CCD camera verified the laser beam, which had an estimated spot size of 2.6 μm, interrogated the irradiated regions. The PL signal was collected by the same objective lens, analyzed by a 50 cm monochromator, and detected with a liquid nitrogen-cooled InGaAs detector. An optical filter was placed at the entrance slit of the monochromator to block any backscattered pump light. Figure 5 shows that for an excitation power of 15 mW, there is quantum dot emission at 1.28 eV and emission from the substrate and cladding layers at 1.5 eV. These results are similar to those found for quantum dots assembled without patterning. For example, regular self-assembled InAs quantum dots had a PL emission at 1.21 eV at 2 K [20] and 7 K [21], and at 1.3 eV for 80 K [22]. Mehta *et al* report similar PL emission for FIB-induced quantum dots, with quantum dot emission at 1.18 eV at 3 mW [23]. From these data we conclude that FIB irradiation does not hinder the PL emission

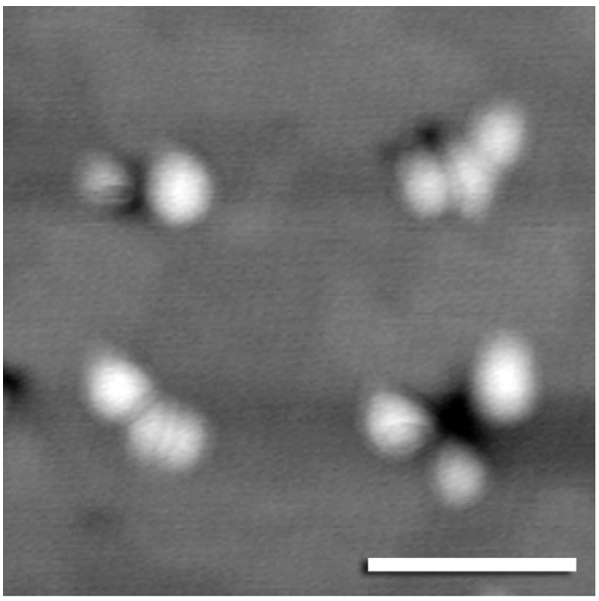

Figure 6. AFM image of a 1.8 ML-thick InAs film upon a pattern of holes spaced 140 nm apart and exposed to the beam 1600 μs per spot. The scale bar is 100 nm and the height scale is 15 nm.

of InAs quantum dots. The width of the peak is likely due to the wide size distribution observed in these samples, which we hope to control by optimizing the patterning process.

It is not surprising that these FIB-induced holes act as nucleation sites in light of the fact that quantum dot formation has been observed on mesa tops [21] and at step edges [24]. In these experiments, quantum dots are not observed away from the pattern until a thickness of 2.2 ML, indicating that the pattern lowers the critical thickness for quantum dot formation [11]. In the case of the FIB-directed assembly observed in these experiments, it is not uncommon for two or three quantum dots to nucleate in the vicinity of a single hole, as seen in the AFM images of figures 4(a) and (b), and the plot in figure 2. The number of locations where at least one quantum dots has formed is consistently less than the number of holes observed for any given dwell time for these growth conditions, suggesting that either some holes are annihilated during the growth of the film, or the AFM is limited in its detection of small dots within the holes. As with the hole arrays, there is no observable effect of the periodicity of the array on the probability of finding one or more dots at a given location for these growth conditions.

The number of quantum dots per hole can be manipulated by altering the growth conditions, namely lowering the growth temperature. Figure 6 shows a high magnification AFM image that shows the details of multiple dot nucleation. In this image, the film is 1.8 ML-thick InAs deposited upon a pattern of holes spaced 140 nm apart with a beam exposure of 1600 μs per spot and a growth temperature of 510 °C. In this lower temperature sample, many smaller dots nucleate at each hole. This is not unexpected, as the nucleation rate is higher at lower temperatures. Furthermore, the lower temperature film is thinner further leading to many small quantum dots.

In order to investigate the nucleation of quantum dots in response to patterned arrays of holes, we employ a kinetic Monte Carlo (KMC) model of crystal growth that take elastic relaxation of the lattice into account. We use a simple solid-on-solid model [25–28] and assume that the migrating surface adatoms are units of GaAs or InAs. In other words, we do not take the effect of As overpressure into account. In this model only surface atoms can move and the hopping rate associated with the pth surface atom is denoted as r_p. The hopping rate is modeled as

$$r_\mathrm{p} = r_0 \exp[(-E_\mathrm{d} - E + \Delta W)/k_\mathrm{B}T]$$

where E_d is the diffusion barrier for InAs on GaAs, $k_\mathrm{B}T$ is the thermal energy, r_0 is the attempt frequency, and E is the composite bonding energy term given by:

$$E = N_\mathrm{GG}\gamma_\mathrm{GG} + N_\mathrm{IG}\gamma_\mathrm{IG} + N_\mathrm{II}\gamma_\mathrm{II} - 5\gamma_\mathrm{IG},$$

N_GG is the total number of GaAs–GaAs bonds between atom p and its nearest and next nearest neighbors and the bond energy is denoted as γ_GG. The quantities N_IG, N_II, γ_IG, and γ_II are defined in an analogous way. (Note: for an isolated InAs atom on a GaAs substrate $E = 0$.) The elastic energy W is given as:

$$\Delta W = W(\text{ with atom p}) - W(\text{ without atom p}).$$

In our simulations we use a ball and spring model with springs connecting nearest and next to nearest neighbors, with spring constants k_L and k_D respectively. W is the total elastic energy and computed by summing the energy of each spring. The computation of ΔW is rather expensive; however one can use the good approximation $\Delta W = \frac{3}{2}w_\mathrm{p}$, where w_p is the

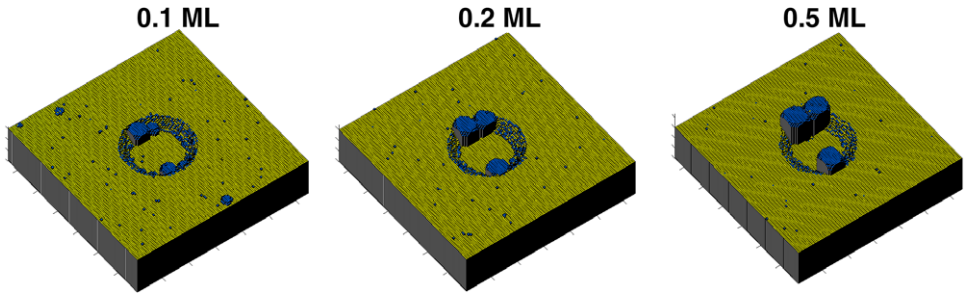

Figure 7. KMC simulation results as a function of deposition of InAs with the same growth parameters and starting morphology. The width of the computational cell is 128 au.

total energy of the springs connected to atom p which is computationally faster. The system is then evolved using rejection-free KMC [29]. After each atom hop the elastic displacement field is updated. This is accomplished using the expanding box method combined with a Fourier multigrid method [28, 30–32].

In these calculations we take the strain of 7% of solid-on-solid cubic crystal substrate (GaAs) and film (InAs), $r_0 = 2 \times 10^{13}$ s^{-1}, $E_d = 1$ eV, $\gamma_{GG} = \gamma_{IG} = .18$ eV, $\gamma_{II} = .16$ eV, $k_L = 62$ eV/a^2, and $k_D = 30$ eV/a^2. The values for γ_{GG}, γ_{IG}, γ_{II}, k_L and k_D were chosen to match the bulk elastic properties of GaAs. These simulations were performed with a 128 atomic units × 128 atomic units (au) matrix, and a height of 30 au. A half monolayer of atoms was deposited and allowed to interact with the buffer layer below, resulting in a three-dimensional morphology.

The simulations qualitatively follow the experimental observations for quantum dot formation. Figure 7 presents the simulated morphology of the film growth as a function of deposited thickness. At the smallest thicknesses (0.1 ML) there are small nuclei on the inner perimeter, with a few small nuclei away from the hole. At higher deposited thickness, the nuclei away from the hole disappear and the nuclei within the perimeter of the hole grow and eventually protrude. It is difficult to determine whether quantum dot growth is accurately observed experimentally because probing the interior of holes of these size scales is hard to achieve with the AFM. The AFM tips have a radius of curvature of 8 nm and can only reliably image protruding dots. Experimentally, the number of locations where quantum dot formation is observed is consistently less than the number of holes observed for any given dwell time (figure 2). The simulations suggest that the holes at which no dots are observed are not necessarily annihilated during the growth of the film; rather, the quantum dots are completely within the holes and are thus undetectable by AFM.

The KMC simulations also replicate experimentally observed formation of quantum dots as a function of growth temperature. A minimum of four runs at different randomizations was used to achieve an average number of dots nucleated per hole. The simulation shows that an increase in the growth temperature from 750 to 850 K severely suppresses the nucleation rate of quantum dots around the patterned hole of 20 au in diameter, from an average of 6.0 ± 1.2 dots to 1.6 ± 0.6 dots (figure 8(a)). This is in reasonable agreement with experimental results that show an average of 4.5 ± 1.2 dots at $T = 510\,^{\circ}$C (783 K) and 1.3 ± 0.6 dots at $T = 530\,^{\circ}$C (803 K) for a dwell time of 1600 μs. Temperature is also a reasonable predictor of whether a quantum dot nucleates away from the patterned hole. At 750 K in the simulations, an average of 2 dots nucleated away from the patterned area and for experimentally grown samples at growth temperatures below 510 °C, AFM reveals more nucleation of quantum dots away from the holes (not shown).

A large distribution in the initial hole diameters, shown as open symbols in figure 3(a), may contribute to the wide distribution in the quantum dot size (closed symbols in figure 3(a)) and multiple dot nucleation at a single hole site,

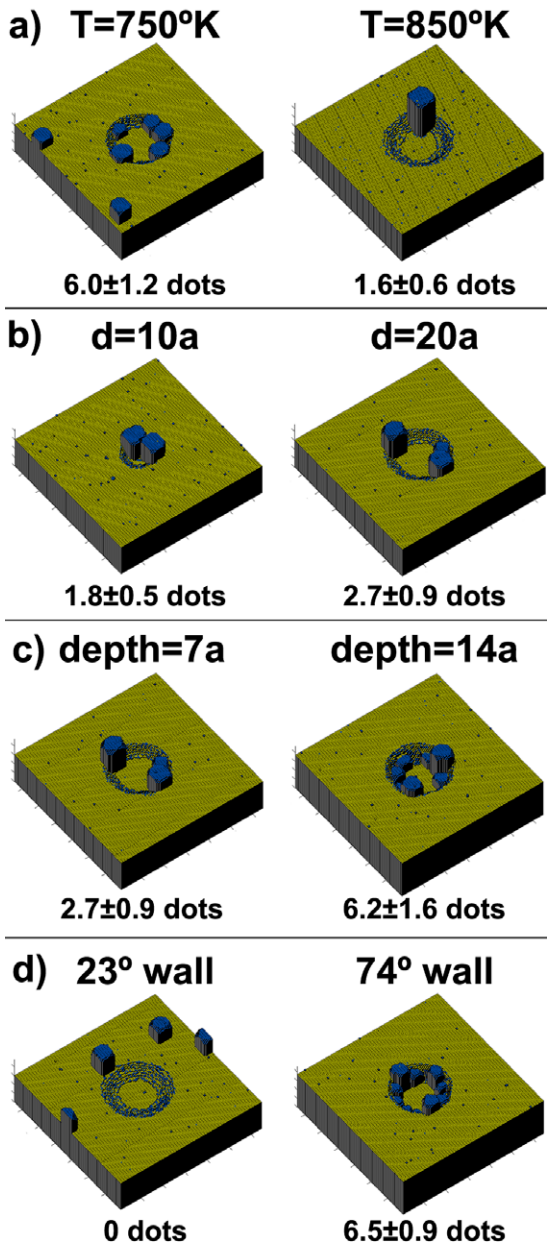

Figure 8. KMC simulation results for (a) varying temperature, (b) varying diameter, (c) varying depth, (d) varying wall slope (gradual = 23°, abrupt = 74° with respect to the surface) of 0.5 ML InAs deposited on GaAs. The number of dots is for an average of at least 4 different randomizations. The width of the computational cell is 128 au.

thus creating the wide PL peak observed in figure 5. From figure 3 it is clear that the diameter and depth change as a function of ion dose, but it is unclear which of these factors influence the number of quantum dots that form. Simulations give us the ability to change one parameter at a time to investigate these effects independently. When the hole diameter was doubled from 10 to 20 au as shown in figure 8(b), the number of quantum dots that formed increased only slightly, 2.1 ± 0.7 to 2.7 ± 0.9 dots, respectively. Instead, simulations show that the driving force of the increasing number of quantum dots per feature seems to be largely

attributed to the depth and slope of the initial hole. Figure 8(c) shows that doubling the depth increases the number of dots nucleating per hole the dots from 2.7 ± 0.9 to 6.2 ± 1.6. Similarly, figure 8(d) shows that when the slope of the hole wall is gradual, 27° with respect to the surface, the dots only nucleate away from the hole. But when the slope is very sharp, 74° with respect to the surface, there are many dots that form within the hole (6.5 ± 0.9). These simulations indicate that the depth and shape of the hole, and not necessarily the diameter, determines the number of quantum dots nucleated.

4. Conclusions

In this work FIB-induced morphologies created self-assembled quantum dots that were optically active. Variations of ion dose and other growth parameters, such as thickness, temperature, geometry of created holes, were examined both experimentally with AFM and also utilizing a KMC simulation with elastic contributions from the buffer layer. Size, fidelity, and the number of dots were strongly influenced by the FIB-irradiated dwell time. At low ion doses, holes are not always present, but increasing the ion dose increases the fidelity and also enlarges the holes. Multiple dots nucleate around a single hole when the temperature is decreased and when the hole surface area increases, i.e. when the hole diameter increases or depth increases.

Acknowledgments

This research was supported in part by a grant from Sandia National Labs (763642). Peter Smereka was supported, in part, by National Science Foundation grants DMS-0553487, DMS-0509124 and DMS-0810113. Thanks to Min W Kim and P C Ku for their assistance with the PL. And a big thank you to Aaron Dehne and Paul Rudzinski for their AFM analysis.

References

[1] Eberl K, Lipinski M O, Manz Y M, Winter W, Jin-Phillipp N Y and Schmidt O G 2001 *11th Int. Winterschool on New Developments in Solid State Physics. Low-Dimensional Systems: Fundamentals and Applications (Feb. 2000)*; *Physica* E **9** 164–74

[2] Livshits D A, Kovsh A R, Maleev N A, Zhukov A E, Ustinov V M, Ledentsov N N, Alferov Z I, Bimberg D, Lin G and Chi J 2003 *Quantum Sensing: Evolution and Revolution from Past to Future (Jan. 2003)*; *Proc. SPIE* **4999** 524–30

[3] Alloing B, Zinoni C, Zwiller V, Li L H, Monat C, Gobet M, Buchs G, Fiore A, Pelucchi E and Kapon E 2005 *Appl. Phys. Lett.* **86** 101908

[4] Ward M B, Karimov O Z, Unitt D C, Yuan Z L, See P, Gevaux D G, Shields A J, Atkinson P and Ritchie D A 2005 *Appl. Phys. Lett.* **86** 201111

[5] Nakamura Y, Schmidt O G, Jin-Phillipp N Y, Kiravittaya S, Muller C, Eberl K, Grabeldinger H and Schweizer H 2002 *J. Cryst. Growth* **242** 339–44

[6] Watanabe S, Pelucchi E, Dwir B, Baier M, Leifer K and Kapon E 2004 *11th Int. Conf. on Modulated Semiconductor Structures (July 2003)*; *Physica* E **21** 193–8

[7] Kiravittaya S, Rastelli A and Schmidt O G 2005 *Appl. Phys. Lett.* **87** 243112

[8] Song H Z, Nakata Y, Okada Y, Miyazawa T, Ohshima T, Takatsu M, Kawabe M and Yokoyama N 2004 *11th Int. Conf. on Modulated Semiconductor Structures (July 2003)*; *Physica* E **21** 625–30

[9] Vandervelde T E, Atha S, Hull R, Pernell T L and Bean J C 2006 *J. Vac. Sci. Technol.* A **24** 375–81

[10] McKay H A, Dehne A, Lee J Y and Millunchick J M 2007 *Appl. Phys. Lett.* **90** 163109

[11] McKay H, Rudzinski P, Dehne A and Millunchick J M 2007 *Nanotechnology* **18** 455303

[12] Kim Y K, Danner A J, Raftery J J and Choquette K D 2005 *IEEE J. Sel. Top. Quantum Electron.* **11** 1292–8

[13] Kitslaar P, Strassner M, Sagnes I, Bourhis E, Lafosse X, Ulysse C, David C, Jede R, Bruchhaus L and Gierak J 2006 *Microelectron. Eng.* **83** 811–4

[14] Menzel R, Bachmann A T and Wesch W 1999 *Nucl. Instrum. Methods Phys. Res.* B **148** 450

[15] Lugstein A, Basnar B and Bertagnolli E 2002 *J. Vac. Sci. Technol.* B **20** 2238–42

[16] Basnar B, Lugstein A, Wanzenboeck H, Langfischer H, Bertagnolli E and Gornik E 2003 *J. Vac. Sci. Technol.* B **21** 927–30

[17] Portavoce A, Kammler M, Hull R, Reuter M C and Ross F M 2006 *Nanotechnology* **17** 4451–5

[18] Yamaguchi K, Kaizu T, Yujobo K and Saito Y 2002 *J. Cryst. Growth* **237–239** 1301–6

[19] Portavoce A, Hull R, Reuter M C and Ross F M 2007 *Phys. Rev.* B **76** 235301

[20] Henini M, Sanguinetti S, Brusaferri L, Grilli E, Guzzi M, Upward M D, Moriarty P and Beton P H 1997 *Microelectron. J.* **28** 933–8

[21] Heitz R, Ramachandran T R, Kalburge A, Xie Q, Mukhametzhanov I, Chen P and Madhukar A 1997 *Phys. Rev. Lett.* **78** 4071–4

[22] Tarasov G G, Mazur Y I, Zhuchenko Z Y, Maassdorf A, Nickel D, Tomm J W, Kissel H, Walther C and Masselink W T 2000 *J. Appl. Phys.* **88** 7162–70

[23] Mehta M, Reuter D, Melnikov A, Wieck A D and Remhof A 2007 *Appl. Phys. Lett.* **91** 123108

[24] Placidi E, Arciprete F, Sessi V, Fanfoni M, Patella F and Balzarotti A 2005 *Appl. Phys. Lett.* **86** 241913

[25] Orr B G, Kessler D A, Snyder C W and Sander L 1992 *Europhys. Lett.* **19** 33

[26] Lam C H, Lee C K and Sander L M 2002 *Phys. Rev. Lett.* **89** 16102

[27] Lung M T, Lam C H and Sander L M 2005 *Phys. Rev. Lett.* **95** 086102

[28] Baskaran A, Devita J P and Smereka P 2009 Kinetic Monte Carlo simulation of strained heteroepitaxial growth with intermixing *Contin. Mech. Thermodyn.* submitted

[29] Blue J L, Beichl I and Sullivan F 1995 *Phys. Rev.* E **51** R867–8

[30] Russo G and Smereka P 2006 *J. Comput. Phys.* **214** 809

[31] Russo G and Smereka P 2006 *Multisc. Model. Simul.* **5** 130

[32] Schulze T P and Smereka P 2009 *J. Mech. Phys. Solids* **57** 521–38